A Finite Volume Approach to NAPL Groundwater Contamination

by

P.A Forsyth

Research Report CS-89-46
October, 1989

A Finite Volume Approach To NAPL Groundwater Contamination

Peter A. Forsyth

Department of Computer Science
University of Waterloo
Waterloo, Ontario N2L 3G1, Canada.

AMS (MOS) Subject Classification: 65MO5, 76505

Keywords: finite volume, Delauney triangulation, positive transmissibilities

Running Title: NAPL contamination

ABSTRACT

Finite difference discretizations of non-aqueous phase liquid (NAPL) groundwater contamination problems ensure that the discrete flux direction is always in the physical direction. This is not always the case for finite element discretizations. If a finite volume approach is used, the above condition is shown to be equivalent to requiring a Delauney triangulation of a two dimensional region (assuming the absolute permeability tensor is constant). A slightly generalized approach can be used for hetrogeneous regions. Use of this type of triangulation is demonstrated for various three phase contamination problems in two dimensions.

1. Introduction

Contamination of groundwater due to non-aqueous phase liquids (NAPL) is a problem of growing concern. Liquids such as PCB's, TCE, dioxins and various petroleum products are known to be leaking from many toxic waste sites [1-10]. It is of interest to track the movement of contaminant in both the saturated and unsaturated zones, so a full three phase solution is required [1,3,4,10]. In many cases, the NAPL solubility in the air phase is small, so that air phase transport can be neglected [3]. With this assumption, the number of equations can be reduced by means of the passive air phase approximation [3,11]. This approximation has been shown to have acceptable accuracy in many practical situations due to the low air pressures involved in near surface flow [11].

Both finite difference [1,3,4,5,9] and finite element [2,7,10] methods have been used to solve this problem. Due to the non-linear hyperbolic nature of the equations, some form of upstream weighting must be used. In the finite difference case, standard upstream techniques can be employed [1,3,4,5,9]. For finite element discretizations, upstream weighted test functions have been devised [2,10,12].

Implicit finite difference techniques produce stable, monotone solutions for complex counter-current flow situations [13,14]. In particular, the discrete equations ensure that saturations are in the physical range (positive and less than one). In the single phase limit, the finite difference pressure equation becomes an M-matrix. This implies that non-physical local maxima and minima in the pressure cannot occur. In the multi-phase case, this corresponds to requiring "positive transmissibilities", or positive flux linkages [15,16]. This means that the direction of the discrete flux always corresponds to the physical direction. This requirement is common in other application areas, such as semi-conductor device modelling [17].

However, finite difference methods have the well known disadvantage of being inflexible when applied to problems with complex geometries. Of course, finite element methods are well suited for situations with non-rectangular geometries.

Unfortunately, upstream weighted finite element discretizations [10,12] will not, in general, yield on M-matrix pressure equation in the single phase limit. This implies (in the multi-phase case) that the discrete flux direction will not always correspond to the physical direction. In addition, it is not clear that the upstream weighted test functions [10,12] ensure that the saturations remain positive.

The objective of this paper is to develop a discretization method for NAPL contamination problems which combines the best features of both techniques. In the following, we will refer to this discretization technique as a finite volume approach. Similar ideas have been suggested by Dalen [18] in the context of reservoir simulation. Finite volume type methods have also been suggested by Potempa [19,20] and Rozen [21], but no attempt was made to ensure that the single phase pressure equation produced an M-matrix. In fact, the basis functions used in references [19-21] rarely produce M-matrices in practical problems. Another possible approach for unstructured grids is based on the integrated finite difference method [22], but this requires that the nodes have a specific geometric placement. Finite volume methods have been used in Navier-Stokes problems and are related to the box method in semi-conductor device modelling [17,23].

In this article, we will develop discrete equations which will always produce saturations in the physical range, regardless of timestep size or mesh size. For a two dimensional problem in a convex domain with a constant permeability tensor, it is possible to use a simple algorithm which will produce a triangulation such that all interior (non-boundary) transmissibilities are positive. No movement or addition of nodes is required. This is possible because of the equivalence of the conditions for positive internal transmissibilities and the definition of a Delauney triangulation [24-26]. Computational results indicate that a slightly generalized algorithm, when applied to non-convex grids with widely varying permeabilities, produces only a small number of negative transmissibilities.

Several example runs are presented, comparing results for discretizations having all positive transmissibilities with results for discretizations having a small number of negative transmissibilities. The tests indicate that macroscopic computed parameters are relatively unaffected by a small number of negative transmissibilities.

In addition, some of the numerical difficulties associated with simulating the movement of dense NAPL contaminants in a hetrogeneous medium will also be described.

2. Formulation

Three phase flow in a porous medium generally requires solution of conservation equations for water (w), air (a) and NAPL (n). However, in keeping with previous work [1,3,4,5,9,10] we will assume that the air phase pressure is constant. Consequently, the liquid saturation can be obtained from the air-NAPL capillary pressure

relation, and the air conservation equation can be eliminated.

The resulting equations are:

Water conservation:

$$\frac{\partial}{\partial t}(\phi \rho_w S_w) = q'_w + \nabla \cdot [\mathbf{K} \rho_w \lambda_w (\nabla P_w - \rho_w g \nabla D)] \tag{1}$$

NAPL conservation:

$$\frac{\partial}{\partial t}(\phi \rho_n S_n) = q'_n + \nabla \cdot [\mathbf{K} \rho_n \lambda_n (\nabla P_n - \rho_n g \nabla D)] \tag{2}$$

where:

S_ℓ = saturation of phase $\ell = n, w$
ϕ = porosity
λ_ℓ = $K_{r\ell} \mu_\ell$
$K_{r\ell}$ = relative permeability of phase ℓ
μ_ℓ = viscosity of phase ℓ
$\mathbf{K}$ = absolute permeability tensor
D = depth
g = gravitational acceleration
P_ℓ = pressure of phase ℓ
ρ_ℓ = density of phase ℓ
q'_ℓ = source/sink term for phase ℓ

In addition to the conservation equations, there are the additional equations:

$$S_n + S_a + S_w = 1 \tag{3}$$

$$P_a = P_n + \alpha P_{can}(S_a) + \{1-\alpha\} [P_{caw}(S_a) - P_{cnw}(S_w = 1)] \tag{4}$$

$$P_n = P_w + \alpha P_{cnw}(S_w) + \{1-\alpha\} P_{cnw}(S_w = 1) \tag{5}$$

where:

$$\alpha = \min(1, S_n / S_n^*) \tag{6}$$

and $P_{can}, P_{cnw}, P_{caw}$ are experimentally determined capillary pressure curves [1]. Note that equations (4-6) have been modified in comparison to the usual capillary pressure relations in reservoir simulation [27]. This is because the usual relations ($\alpha=1$) do not produce the correct limit as S_n goes to zero [3,10]. The usual relations implicity assume the existence of a continuous non-aqueous phase. This assumption is clearly invalid in groundwater contamination problems since S_n is usually zero initially. If S_n^* in equation (6) is equal to the critical oil saturation, then equations (4-6) are correct in both limits of vanishing S_n, and for a continuous NAPL phase.

Note that since P_a (air pressure) is assumed constant, then equation (4) can be solved for S_a, so that:

$$S_a = (1 - S_n - S_w) = f(P_n) \tag{7}$$

which differs from the usual reservoir simulation case. The three phase relative permeability for NAPL (K_{rn}) is given by Stone's model [27].

3. Discretization

To avoid obscuring the basic ideas, we will first discretize the model equation:

$$\frac{\partial S}{\partial t} = \nabla \cdot [\mathbf{K} \lambda(S) \nabla P] \tag{8}$$

which can be regarded as prototypical of equation (1-2). Let N_i be the usual C^0 finite element polynomial basis functions [28] where:

$$\begin{aligned} N_i &= 1 \text{ at node } i \\ &= 0 \text{ at all other nodes} \\ \sum_i N_i &= 1 \text{ everywhere in the domain} \end{aligned} \tag{9}$$

We have not, as yet, specified the element geometry, or the type of basis function.

Let:

$$P = \sum_i P_i N_i \tag{10}$$

Using a lumped mass approach for the time derivative term of equation (8), and a Galerkin approximation for the divergence term gives:

$$\frac{S_i^{N+1}-S_i^N}{\Delta t}\int_v N_i\,dv \tag{11}$$

$$=-\int_v \mathbf{K}[\lambda(S)\nabla P\cdot\nabla N_i]\,dv$$

where v is the volume of the region of interest, superscript N is the time level, and Δt is the time increment. We will leave as unspecified the time level of evaluation of the right hand side of equation (11) for the time being. Anticipating the use of some form of upstream weighting for $\lambda(S)$, the integral in the right hand side of equation (11) is approximated by:

$$-\int_v (\mathbf{K}\nabla P\cdot\nabla N_i)\lambda(S)\ dv \tag{12}$$

$$\approx -\lambda(S^*)\int_v \mathbf{K}\nabla P\cdot\nabla N_i\ dv$$

where S^* is some as yet unspecified point in the support of N_i. The above approximation avoids costly numerical integration during construction of the Jacobian, and is sometimes called the influence coefficent technique [29,30].

It follows from equation (9) that:

$$-\int_v \mathbf{K}\nabla P\cdot\nabla N_i\ dv \tag{13}$$

$$=\sum_{j\in\eta_i}\gamma_{ij}\ (P_j-P_i)$$

where:

$$\gamma_{ij}=-\int_v \mathbf{K}\nabla N_j\cdot\nabla N_i\ dv \tag{14}$$

Here η_i is the set of neighbour nodes of node i. Letting V_i be the volume associated with node i:

$$V_i=\int_v N_i\ dv \tag{15}$$

then an upstream weighted discretization of equation (8) can be defined by:

$$\left(\frac{S_i^{N+1}-S_i^N}{\Delta t}\right)V_i=\sum_{j\in\eta_i}\lambda_{ij}^{ups}\,\gamma_{ij}(P_j-P_i) \tag{16}$$

where:

$$\lambda_{ij}^{ups}=\lambda_j \quad \text{if}\gamma_{ij}(P_j-P_{i)})>0 \qquad (17)$$
$$=\lambda_i \quad \text{if } \gamma_{ij}(P_j-P_{i)})<0$$

Since γ_{ij} (equation (14)) is symmetric, then equation (16) is mass conservative. Using the same approach, equations (1-2) can be discretized in a similar manner:

Water equation:

$$\frac{V_i}{\Delta t}[(\phi\rho_w S_w)_i^{N+1}-(\phi\rho_w S_w)_i^N] \qquad (18)$$
$$=q_{w,i}^{N+1}+\sum_{j\in\eta_i}\gamma_{ij}(\lambda_w^M\rho_w^M)_{ij}^{ups}\psi_{w,ij}$$

where:

$$\psi_{w,ij}=(P_{n,j}^{N+1}-P_{n,i}^{N+1})-(P'_{cnw,j}-P'_{cnw,i})^M$$
$$-\rho_{w,ij+½}\ g(D_j-D_i)$$
$$P'_{cnw}=P_n-P_w \quad \text{(see equation (5))}$$

NAPL equation:

$$\frac{V_i}{\Delta t}[(\phi\rho_n S_n)_i^{N+1}-(\phi\rho_n S_n)_i^N] \qquad (19)$$
$$=q_{n,i}^{N+1}+\sum_{j\in\eta_i}\gamma_{ij}(\lambda_n^M\ \rho_n^M)_{ij}^{ups}\ \psi_{n,ij}$$

where:

$$\psi_{n,ij}=(P_{n,j}^{N+1}-P_{n,i}^{N+1})-\rho_{n,ij+½}\ g\,(D_j-D_i)$$

and

$$q_\ell=q'_\ell\ V_i \qquad (20)$$
$$\lambda_w^M=\lambda_w\ (P_n^{N+1},\ S_n^M)$$
$$\lambda_n^M=\lambda_n\ (S_n^M)$$
$$\rho_{\ell,ij+½}=(\rho_{\ell,j}+\rho_{\ell,i})/2$$

$$(\lambda_\ell\ \rho_\ell)_{ij}^{ups}=(\lambda_\ell \rho_\ell)_i \quad \text{if} \quad \gamma_{i,j}\ \psi_{\ell,ij}<0$$
$$=(\lambda_\ell\ \rho_\ell)_j \quad \text{if} \quad \gamma_{ij}\ \psi_{\ell,ij}>0$$

When $M=N+1$ in equations (18) and (19), a fully implicit time discretization is used, while if $M=N$, an IMPES types method is defined. Allowing M to vary from node to node defines an adaptive implicit scheme [14,31], which will be used in the following. The non-linear algebraic equations (18, 19) are solved using full Newton iteration. If $(P_{n,i},\ S_{n,i})$ are the primary variables for each node (i.e. those variables which are regarded as independent when constructing the Jacobian), and if

$$\frac{d\lambda_n}{dS_n}\ (S_n=0)=0 \tag{21}$$

then there will be no timestep restriction for an IMPES discretization in those regions where $S_n \equiv 0$. This is because if equation (21) holds, then when $S_n \equiv 0$, a Newton iterative procedure for solving equations (18-19) is equivalent to Newton iterative solution of a discrete form of Richards equation [32] for unsaturated flow. This is solved fully implicitly for P_n (recall that $P_n=P_w+$ constant when $S_n=0$). Consequently, if an adaptive implicit method is used, then the computational work in regions with $S_n=0$ is comparable to a fully implicit solution of Richards equation.

Analysis of equations (18-19) reveals that, if a fully implicit method is used, it is not possible to solve the algebraic equations unless:

$$S_n^{N+1},\ S_w^{N+1} \in [0,\ 1]$$

assuming

$$\lambda_n=0 \quad \text{if} \quad S_n \leq 0 \tag{22}$$
$$\lambda_w=0 \quad \text{if} \quad S_w \leq 0$$

The same statement is true for an IMPES method for a sufficiently small timestep.

In the case of saturated flow $(S_a=0)$, then using the techniques of reference [14], it can easily be shown that equations (18-19) are monotone in S_n if the appropriate conditions hold [14].

4. Positive Transmissibility Condition

The condition for positive transmissibilities is (from equation (13) and equations (18-19)):

$$\gamma_{ij} \geq 0 \quad \forall\ i,j \tag{23}$$

It is instructive at this point to consider some typical two dimensional basis functions. One possible choice consists of C^0 piecewise bilinear functions defined on quadrilaterals. However, this is a poor choice if condition (23) is desired.

To see this, consider a problem where $\mathbf{K}$ is constant. The algebraic influence of $\mathbf{K}$ in equation (14) can be eliminated by defining an (x', y') co-ordinate system such that $\mathbf{K}'=\mathbf{I}$ in this new system. This is always possible since $\mathbf{K}$ is symmetric positive definite. If the elements are rectangles with:

$$\begin{aligned} \triangle x' &= x'_{i+1} - x'_i \\ \triangle y' &= y'_{j+1} - y'_j \end{aligned} \tag{24}$$

then some straightforward algebra shows that condition (23) is violated unless:

$$\max \left\{ \frac{\triangle x'}{\triangle y'}\ ,\ \frac{\triangle y'}{\triangle x'} \right\} \leq \sqrt{2} \tag{25}$$

For definiteness, if we assume that:

$$\mathbf{K} = \begin{bmatrix} K_x & 0 \\ 0 & K_y \end{bmatrix}$$

and that x is the horizontal direction, and y is the vertical direction (depth), then equation (25) implies (in the original (x,y) co-ordinate system):

$$\frac{\triangle x}{\triangle y} \leq (2K_x/K_y)^{1/2}. \tag{26}$$

In typical contamination problems, condition (26) is not met by a large margin, since horizontal distances are typically an order of magnitude larger than vertical distances.

Another possible choice for C^0 basis functions are piecewise linear functions defined on triangles. Again, consider the (x',y') system so that $\mathbf{K}'=\mathbf{I}$. An arbitrary arrangement of nodes may be used. For an interior edge, as shown in Figure 1, some simple geometry shows that condition (23) is satisfied if and only if [33]:

$$\alpha+\beta \leq \pi \tag{27}$$

For a boundary edge, condition (26) requires that the angle opposite the edge is less than $\pi/2$. (All these angles are measured in the (x',y') co-ordinate system).

In practical problems, the internal nodes are often placed to correspond with layers of rock or soil having different properties. Therefore, it is inappropriate to attempt to satisfy condition (23) by movement of internal nodes. We would also like to avoid adding extra internal nodes.

However, condition (27) for interior nodes is equivalent to specifying a Delauney triangulation [25]. An interesting result concerning Delauney triangulations is that, for convex regions, a Delauney triangulation can be produced from any valid triangulation [34] by a series of local edge swaps [25]. This local edge swap procedure is illustrated in Figure 2. Given a valid triangulation, an edge such as AC is examined. If the sum of the angles opposite this edge is greater that π, then this edge is replaced by DB. This edge swap can, of course, only be carried out if $ABCD$ (Figure 2) is convex. If $ABCD$ is not convex, then necessarily $(\alpha+\beta)$ (Figure 1) must be less than π. In general, this will disturb the edges of the polygon $ABCD$ (Figure 2), and these edges must be re-examined. However, this sequence of local edge swaps eventually converges to a Delauney triangulation.

For our purposes, we generalize the edge swap criteria as follows: an edge AC is examined, and the transmissbility γ_{AC} is determined by carrying out the integration in equation (14). If γ_{AB} is negative, then replace this edge by DB, and continue. If the region is convex, and $\mathbf{K}$ is constant, this procedure is equivalent to finding the Delauney triangulation in the (x',y') plane where $\mathbf{K}'=\mathbf{I}$, and hence must converge. (Note that a valid edge swap in the (x',y') plane is a valid edge swap in the (x,y) plane since convex polygons in the (x',y') plane are convex polygons in the (x,y) plane).

In general, for non-convex regions or non-constant $\mathbf{K}$, this procedure may not produce a triangulation such that equation (23) is satisfied for all internal edges. However, since most regions which arise in practice can be thought of as a union of convex regions with constant $\mathbf{K}$ plus some interface regions, this local edge swap procedure should tend to minimize the number of internal edges having negative transmissibilities. In practice, to avoid any possible cycling, we limit the number of edge swaps allowed.

Even for convex regions with constant $\mathbf{K}$, it is possible to end up with edges on the boundaries which have negative transmissibilities. (There is no possible edge swap for a boundary edge). We can try to eliminate this problem by adding a boundary node as in Figure 3. Suppose edge AB has $\gamma_{AB} < 0$. This implies that in the $(x'y')$ plane, the angle opposite edge AB is greater than $\pi/2$. A new node is added at the intersection of AB with the perpendicular to AB drawn from C (this is all carried out in the (x',y') plane). This procedure will be described as boundary node addition.

It seems extremely unlikely that any higher order basis functions will give rise to any reasonable criteria which will satisfy equation (23). Consequently, in the following, we will restrict attention to two dimensional linear basis functions defined on triangles.

5. DNAPL Contamination in a Homogeneous Region

The first example consists of a NAPL contaminant which is denser than water (DNAPL specific gravity = 1.2). The homogeneous region for this problem is shown in Figure 4. In this particular example, we expect that the DNAPL will sink through the unsaturated zone above the water table, through the saturated zone, until encountering the no-flow bottom boundary. The contaminant should then flow along the boundary until leaving the region through the constant pressure edges (the pressure at the side boundaries is set to the hydrostatic pressure of water, as shown in Figure 4). A detailed description of the data for this example is given in the Appendix.

Two levels of grids will be used in the following: a coarse grid and a fine grid which is constructed from the coarse grid by joining the midpoints of the sides of the coarse grid triangulation (see Figure 5).

In order to investigate the effect of a small number of negative transmissibility edges, we will also use two approaches to producing a coarse grid triangulation. The first technique uses local edge swapping and boundary node addition to ensure that all edges have positive transmissibility. The second technique does not add boundary nodes.

Figure 6a shows the fine grid without boundary node addition (1089 nodes) and Figure 6b shows the fine grid with boundary node addition (1161 nodes). The grid in Figure 6a has 16 out of 2379 edges with negative transmissibilities. These negative transmissibilities all occur on either the top or bottom boundary, near the location of the extra boundary nodes (near solid colour in Figure 6b). Figure 6b has no negative transmissibility edges.

Consequently, any difference between computations on the two grids should be apparent when the DNAPL flows along the bottom edge, between 20 and 30 m from the origin. In particular, we expect to observe the phenomena shown in Figure 7. If edge AB is a boundary edge, then physically a dense fluid will flow along the path from A to B. However, if AB has a negative transmissibility, then a dense fluid must first flow from A to C, and then from C to B. Of course, for a very fine grid, we expect that this non-physical flow path will have a vanishingly small effect. However, it remains to be seen if this non-physical behaviour has an observable effect on coarse

grids.

The contamination problem of Figure 4 was first initialized in an arbitrary state, and then allowed to run for one year with no DNAPL injection. This produced a steady state water saturation profile. After the first year, DNAPL was injected at the site indicated for one year (see Figure 4).

Figure 8 shows the DNAPL saturation values after one year of injection, for both coarse grids. Figure 8a shows results for the grid with negative transmissibilities along the bottom boundary, while Figure 8b shows the results for the coarse grid with all positive transmissibilities. The somewhat ragged appearance of the interface between zones having different S_n levels is magnified by the shading algorithm, which shades the control volumes associated with each node.

A detailed examination of the results reveals that the non-physical flow path phenomena described in Figure 7 does occur for the grid with negative transmissibilities. This small effect can be seen by comparing Figure 8a to Figure 8b (along the lower boundary from 20 to 30 m). Figure 9 shows the fine grid results for both types of grids. As expected, the interface zones become smoother as the grid is refined, and the graphs (Figure 9a and 9b) become quite similar.

A more quantitative description of the difference between computations for the two grid types (as shown in Figure 6) is given in Table 1. This table shows the amount of DNAPL remaining in the system after one year. The discretization error for this macroscopic quantity is about 3%, which would certainly be adequate accuracy in any practical problem. Note that the differences in DNAPL retention for the grids of Figures 6a and 6b are less than the level of discretization error.

Clearly, there is a small observable effect on computational results due to negative transmissibilities. However, if the number of edges having negative transmissibilities is small, then the effect on macroscopic parameters is also small. Either computation using the grid of Figure 6a or Figure 6b is acceptable. However, since the boundary node addition procedure sometimes adds nodes which are quite close to existing nodes, this generally causes more Newton iterations. (Closely spaced nodes will produce nodes with small effective volumes). Consequently, more computational work is required for a grid where condition (23) is always true. Of course, this problem of closely spaced nodes can be alleviated by some type of node movement, but, as discussed in the Introduction, we have excluded this possibility from consideration.

6. LNAPL Contamination in a Homogeneous Region

As a second example, the same problem as defined in Section 5 was run with a specific gravity of NAPL set to .95. In this light NAPL (LNAPL) scenario, we expect that the LNAPL will tend to float on the water table, and have less tendency to penetrate the aquifer, compared to the DNAPL case.

Figure 10 shows the NAPL saturation values after one year of injection. Figure 10a corresponds to the coarse grid version of the grid shown in Figure 6a, while Figure 10b corresponds to the coarse grid version of Figure 6b. As expected, the highest saturation values "sit" on top of the water table. However, the contaminant does penetrate quite far into the aquifer. This is due to the head of NAPL in the unsaturated zone (the capillary fringe is quite narrow). Figure 11 shows the fine grid results corresponding to Figure 10. Examination of these graphs shows that there is little difference between Figures 10a and 10b, and between Figures 11a and 11b. This indicates, once again, that a small number of edges with negative transmissibilities is quite acceptable.

7. DNAPL Contamination in a Hetrogeneous Region

An example of a hetrogeneous region is shown in Figure 12 and 13. The High-P_c region in Figure 13 has nodes which use a different capillary pressure table than used elsewhere. This High-P_c zone is considered to consist of a porous medium with a large NAPL-water capillary pressure. Regions with a large capillary pressure can be effective at blocking NAPL flow [35].

The absolute permeability is isotropic everywhere, and K=1000 md except in the designated zones shown in Figure 13, where K=.1 md. Complete details of the data for this problem are given in the Appendix.

The fine grid discretization for this problem is shown in Figure 14. The edge swapping procedure produced a final discretization with no negative transmissibilities.

This example was initially allowed to run for one year with no DNAPL injection, in order to obtain a steady state profile. DNAPL was injected for one year, and then DNAPL injection ceased while water injection (rain fall) continued for another two years.

The DNAPL saturation profiles are shown in Figure 15 for both coarse (400 nodes) and fine (1521 nodes) grids. It is clear that hetrogeneous systems result in very complex contaminant motion. Since hetrogeneous systems are typical of actual sites [2, 3, 35], DNAPL contaminant will tend to be dispersed over large areas. This will make

site remediation and clean-up very difficult, due to the large volumes contaminated with low saturation (and hence almost immobile) DNAPL.

Note that the high S_n profile ($S_n > .5$) is quite jagged at the bottom of the High-P_c zone in Figure 15b. This is because all the input date are specified on the coarse grid, and interpolated onto the fine grid. In the case of the P_c tables, the default table was used for fine grid nodes unless all coarse grid nodes neighbouring fine grid noes were in the high P_c region. This had the effect of magnifying the staircase pattern present on the coarse grid.

For all the example runs, no particular difficulty was observed with the iterative solver, which was a reduced system/ILU type [36], even for the grids containing some negative transmissibilities.

Many experiments were carried out on various grids having hetrogeneous properties. In all cases, the edge swapping procedure and boundary node addition produced triangulations with only a small number of negative transmissibilities, compared to the total number of edges.

8. Conclusions

Previous attempts to use finite volume methods for unstructured grid multi-phase flow problems did not ensure that positive transmissibilities resulted from a given node placement. This can have undesirable consequences, since the discrete fluid motion follows a non-physical flow path. It is also possible that non-physical local maxima and minima may appear in the pressure field.

In two dimensions, bilinear basis functions defined on quadrilaterials are inappropriate for geometries of interest. However, for convex regions with a constant permeability tensor, use of C^0 linear triangular basis functions, combined with the edge swapping algorithm suggested in this work, guarantees that all internal edges have positive transmissibilities. This procedure does not require any node movement. Possible negative transmissibilities at boundary edges can be removed by adding suitably placed boundary nodes.

In the general case of non-convex, hetrogeneous problems which arise in practice, it is probably not possible to eliminate all negative transmissibilities without node movement. However, various tests indicated that the edge swapping algorithm reduced the occurance of negative transmissibility edges to a small fraction of the total number of edges. In all cases (positive or negative transmissibilities) the selection of the upstream point ensures that the solution of the implicit discrete equations forces the

saturations to lie in the physically relevant range.

Test computations were carried out on some NAPL contamination problems using a grid having all positive transmissibilities and a similar grid having a small number of negative transmissibilities. Although there was a small observable effect on computational results for nodes having negative transmissibilities, there was little difference in macroscopic parameters. This indicates that a grid with a small number of negative transmissibility edges is acceptable for practical problems. Such a grid can be produced using the edge swapping algorithm. Of course, care should be taken to ensure that nodes which correspond to wells, for example, should not have any negative transmissibilities.

Comparison of results on the two types of grids also seemed to indicate that a small number of negative transmissibilities did not adversely affect the Newton iteration, or the iterative matrix solver.

However, DNAPL contamination problems are fairly difficult to solve numerically, due to the rapid downward movement of DNAPL. The highly non-linear capillary pressure relations, which determine the liquid saturation under the passive air phase assumptions, also tend to give the Newton iteration some difficulty. Of course, these problems are present regardless of the discretization scheme used.

The finite volume discretization technique described in this work can be applied to fully three dimensional unstructured grids. In order to avoid negative transmissibilities, the obvious choice would be C^0 linear tetrahedral elements. It is possible to generalize the idea of a Delauney triangulation to a three dimensional tetrahedral tesselation. The three dimensional Delauney tesselation can be obtained by a series of local edge swaps [26]. However, it is not known if a three dimensional Delauney tesselation necessarily results in a grid having all positive transmissibilities.

Appendix

This appendix contains the details of the input data for the homogeneous and hetrogeneous examples.

Table 2 shows the data for the homogeneous DNAPL example. The same physical data was also used for the LNAPL case. Table 3 gives the relative permeability and capillary pressure data.

The hetrogeneous problem used the same physical data as in Table 2. The relative permeability and capillary pressure data were the same as used for the homogeneous problems (Table 3), except for the high-P_c zones as indicated in Figure 13. For

the high-P_c zones, the data given in Table 4 was used.

In all cases, three phase relative permeabilities were computed using Stone's second method [27].

References

[1] C. Faust, "Transport of immiscible fluids within and below the unsaturated zone," Water Res. Res., 21 (1985) 587-596.

[2] M. Osbourne, J. Sykes, "Numerical modelling of immiscible organic transport in the Hyde Park landfill," Water Res. Res., 22 (1986) 25-33.

[3] L.M. Abriola, G.F. Pinder, "A multiphase approach to the modelling of porous media contamination by organic compunds 1. Equation development," Water Res. Res., 21 (1985) 11-18.

[4] L.M. Abriola, G.F. Pinder, "A multiphase approach to the modelling of porous media contamination by organic compounds 2. Numerical simulation," Water Res. Res., 21 (1985) 19-26.

[5] G.F. Pinder, L.M. Abriola, "On the simulation of nonaqueous phase organic compounds in the subsurface," Water Res. Res. 22 (1986) 109S-119S.

[6] A.L. Baehr, M.Y.A. Corapcioglu, "A compositional multiphase model for groundwater contamination by petroleum products 2. Numerical solution," Water Res. Res. 23 (1987) 201-213.

[7] D.P. Hochmuth, D.K. Sunada, "Groundwater model of two phase immiscible flow in coarse material," Groundwater 23 (1985) 617-626.

[8] T. Kuppusamy, J. Sheng, J. Parker, R. Lehhard, "Finite element analysis of multiphase immiscible flow through soils," Water Res. Res. 23 (1987) 625-631.

[9] P.A. Forsyth, "Simulation of nonaqueous phase groundwater contamination," Adv. Water Res. 11 (1988) 74-83.

[10] J. Kaluarachchi, J. Parker, "An efficent finite element method for modelling multiphase flow," Water Res. Res. 25 (1989) 43-54.

[11] P.A. Forsyth, "Comparison of the single phase and two phase numerical model formulation for saturated-unsaturated groundwater flow," Comp. Meth. Appl. Mech. Eng. 69 (1988) 243-259.

[12] P.S. Huyakorn, G.F. Pinder, "A new finite element technique for the solution of two-phase flow through porous media," Adv. Water Res. 5 (1978) 285-298.

[13] P.H. Sammon, "An analysis of upstream differencing," Soc. Pet. Engrg. J. Res. Engrg. 3 (1988) 1053-1056.

[14] P.A. Forsyth, "Adaptive implicit criteria for two-phase flow with gravity and capillary pressure," SIAM J. Sci. Stat. Comp. 10 (1989) 227-252.

[15] C. Prakesh, "Examination of the upwind formulation in the control volume finite element method for fluid flow and heat transfer," Num. Heat Transfer 11 (1987) 401-416.

[16] G. Schneider, M.J. Raw, "A skewed, positive influence coefficent upwinding procedure for control volume based finite element convection diffusion computation," Num. Heat Transfer 9 (1986) 1-26.

[17] C.S. Rafferty, M. Pinto, R.W. Dutton, "Iterative methods in semiconductor device simulation," IEEE Trans. on Computer-Aided Design CAD-4, No. 4 (October-1985) 462-471.

[18] V. Dalen, "Simplified finite-element models for reservoir flow problems," Soc. Pet. Engrg. J. (Oct.-1979) 333-343.

[19] T. Potempa, "A numerical model of two dimensional, two component, single phase miscible displacement in a porous medium," SIAM J. Sci. Stat. Comp. 6 (1985) 582-598.

[20] T. Potempa, "Mobility weighting in numercial reservoir simulation," Soc. Pet. Engrg. J. 25 (1985) 565-572.

[21] B. Rozen, "A generalized finite volume discretization method for reservoir simulation," paper SPE 18414, presented at the Tenth SPE Symposium on Reservoir Simulation, Houston, 1989.

[22] Z. Heinemann, C. Brand, "Modeling reservoir geometry with irregular grids," paper SPE 18412, presented at the Tenth SPE Symposium on Reservoir Simulation, Houston, 1989.

[23] R. Bank, D. Rose, "Some error estimates for the box method," SIAM J. Num. Anal. 24 (1987) 777-787.

[24] R. Sibson, "Locally eqiangular triangulations," Computer J. 21 (1978) 243-245.

[25] B. Joe, "Delauney triangular meshes in convex polygons," SIAM J. Sci. Stat. Comp. 7 (1986) 514-539.

[26] B. Joe, "Delauney triangulations from local transformations," SIAM J. Sci. Stat. Comp. 10 (1989) 718-741.

[27] K. Aziz, A. Settari, "Petroleum reservoir simulation," Applied Science, London, 1979.

[28] O. Axelsson, V. Barker, "Finite element solution of boundary value problems," Academic Press, Toronto, 1984.

[29] P.S. Huyakorn, S.D. Thomas, B.M Thompson, "Techniques for making finite elements competitive in modeling flow in variably saturated porous media," Water Res. Res. 20 (1984) 1099-1115.

[30] P.S. Huaykorn, E.P. Springer, V. Guvanasen, T.D. Wadsworth, "A three dimensional finite element model for simulating water flow in variably saturated porous media," Water Res. Res. 22 (1986) 1790-1808.

[31] P.A. Forsyth, P.H. Sammon, "Practical considerations for adaptive implicit methods in reservoir simulation," J. Comp. Phys. 62 (1986) 265-281.

[32] R.A. Freeze, J.A. Cherry, "Groundwater", Prentice-Hall, Englewood Cliffs, NJ, 1979.

[33] P.A. Forsyth, "A control volume finite element method for local mesh refinement," paper SPE 18415, presented at the Tenth SPE Symposium on Reservoir Simulation, Houston, 1989.

[34] R.B. Simpson, "A two dimensional mesh verification algorithm," SIAM J. Sci. Stat. Comp. 2 (1981) 455-473.

[35] S. Feenstra, J.A. Cherry, "Subsurface contamination by dense non-aqueous phase liquid (DNAPL) chemicals at Tyson's site, Montgomergy County, Pennsylvania: Concepts and Implications," Zenon Environmental Inc., 1986.

[36] G. Behie, P.A. Forsyth, "Incomplete factorization methods for fully implicit simulation of enhanced oil recovery," SIAM J. Sci. Stat. Comp. 5 (1984) 543-561.

TABLE 1

Amount of DNAPL remaining in the system after one year (10 m^3 injected, homogeneous example).

	DNAPL Volume (m^3)	
	Coarse Grid	**Fine Grid**
Some negative transmissibilities (Figure 6a)	7.26	7.05
All positive transmissibilities (Figure 6b)	7.38	7.13

TABLE 2

Physical data for the homogeneous examples. The same data was used for the hetrogeneous example, except where indicated in Figure 13.

Absolute permeability ($K_x = K_y = K_z$)	$10^{-12} m^2$
Porosity, ϕ	.3
Densities	$\rho_w = 1000\ Kg/m^3$
	ρ_n (DNAPL) $= 1200\ Kg/m^3$
	ρ_n (LNAPL) $= 950\ Kg/m^3$
Viscosities	$\mu_w = 1.0$ cp
	$\mu_n = 1.0$ cp

TABLE 3

Relative permeability and capillary pressure tables, used in the homogeneous examples, and everywhere except as indicated in Figure 13 for the hetrogeneous example.

NAPL-Water Data

S_w	K_{rw}	K_{rn}	P_{cnw} (Kpa)
.2	0.0	.68	9.0
.3	.04	.55	5.4
.4	.10	.43	3.9
.5	.18	.31	3.3
.6	.30	.20	3.0
.7	.44	.12	2.7
.8	.60	.05	2.4
.9	.80	0.0	1.5
1.0	1.0	0.0	0.0

Liquid-Air Data

$(1-S_a)$	K_{ra}	K_{rna}	P_{can} (Kpa)	P_{caw} (Kpa)
.2	.64	0.0	9.0	6.6
.32	.46	0.0	3.0	4.5
.40	.36	.0009	.24	3.9
.50	.25	.045	2.1	3.6
.60	.16	.116	1.8	3.3
.70	.09	.210	1.5	3.0
.80	.04	.34	1.2	2.0
.90	.01	.49	.90	1.0
1.0	0.0	.68	0.0	0.0

$S_n^* = .1$ (see equation (6))

TABLE 4

Relative permeability and capillary pressure data for the high-P_c zone in the hetrogeneous problem (Figure 13)

TABLE 4

S_w	K_{rw}	K_{rn}	P_{cnw} (Kpa)
.2	0.0	.68	50.0
.3	.04	.55	30.0
.4	.10	.43	20.0
.5	.18	.31	15.0
.6	.30	.20	13.0
.7	.44	.12	12.0
.8	.60	.05	11.0
.9	.80	0.0	10.5
1.0	1.0	0.0	10.0

Liquid-Air Data

$(1-S_a)$	K_{ra}	K_{rna}	P_{can} (Kpa)	P_{cnw} (Kpa)
.2	.64	0.0	10.0	10.0
.32	.46	0.0	5.0	5.0
.40	.36	.0009	4.5	4.5
.50	.25	.045	4.0	4.0
.60	.16	.116	3.5	3.5
.70	.09	.210	3.0	3.0
.80	.04	.34	2.0	2.0
.90	.01	.49	1.0	1.0
1.0	0.0	.68	0.0	0.0

$S_n^* = .1$ (see equation (6))

Figure Captions

(1) Quadrilateral formed by the two internal triangles which have a common edge.

(2) Local edge swap procedure: replace AC by DB.

(3) Boundary node addition procedure for a boundary edge.

(4) Domain for DNAPL and LNAPL contaminant examples in a homogeneous region.

(5) Method for constructing a fine triangulation (dotted plus solid lines) from a coarse triangulation (solid line only).

(6) Triangulation for domain of Figure 4

- (a) 1089 nodes (some negative transmissibilities)
- (b) 1161 nodes (all positive transmissibilities). Solid colour indicates high density triangulation near extra boundary nodes.

(7) Physical flow path (AC) and discrete flow path ($AB-BC$) when AC has a negative transmissibility.

(8) DNAPL saturation values after one year (coarse grid)

- (a) some negative transmissibilities (289 nodes)
- (b) all positive transmissibilities (309 nodes).

(9) DNAPL saturation values after one year (fine grid)

- (a) some negative transmissibilities (1089 nodes)
- (b) all positive transmissibilities (1161 nodes).

(10) LNAPL saturation values after one year (coarse grid)

- (a) some negative transmissibilities (289 nodes)
- (b) all positive transmissibilities (309 nodes).

(11) LNAPL saturation values after one year (fine grid)

(a) some negative transmissibilities (1089 nodes)

(b) all positive transmissibilities (1161 nodes).

(12) Domain of DNAPL hetrogeneous problem.

(13) Details of hetrogeneities for Figure 12.

(14) Fine grid triangulation for Figure 12 (1521 nodes).

(15) DNAPL saturation values, hetrogeneous problem, after two years

(a) coarse grid (400 nodes)

(b) fine grid (1521 nodes).

FIGURE 1

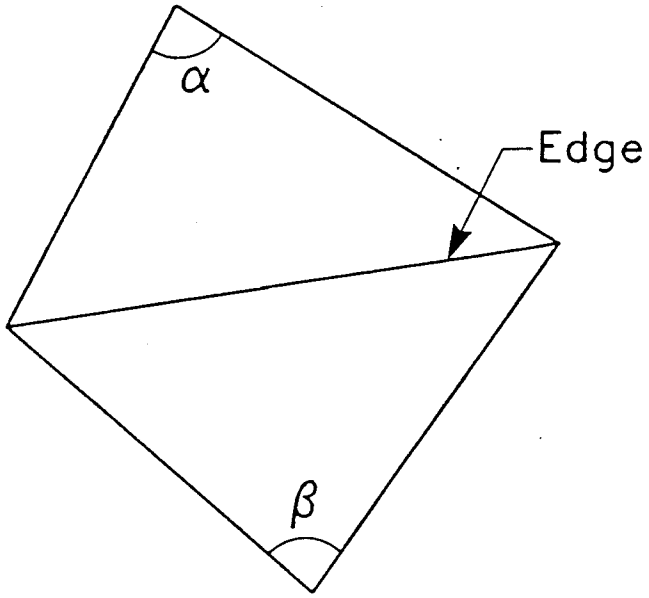

Quadrilateral formed by the two internal triangles which have a common edge.

FIGURE 2

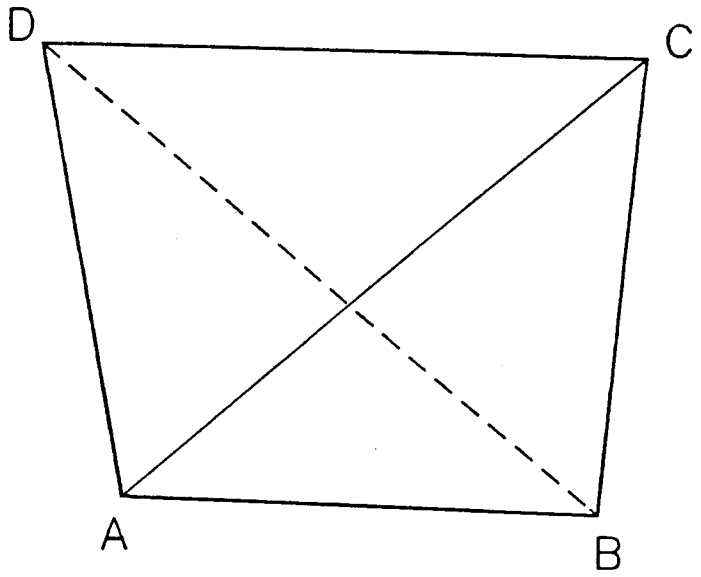

Local edge swap procedure: replace AC by DB.

FIGURE 3

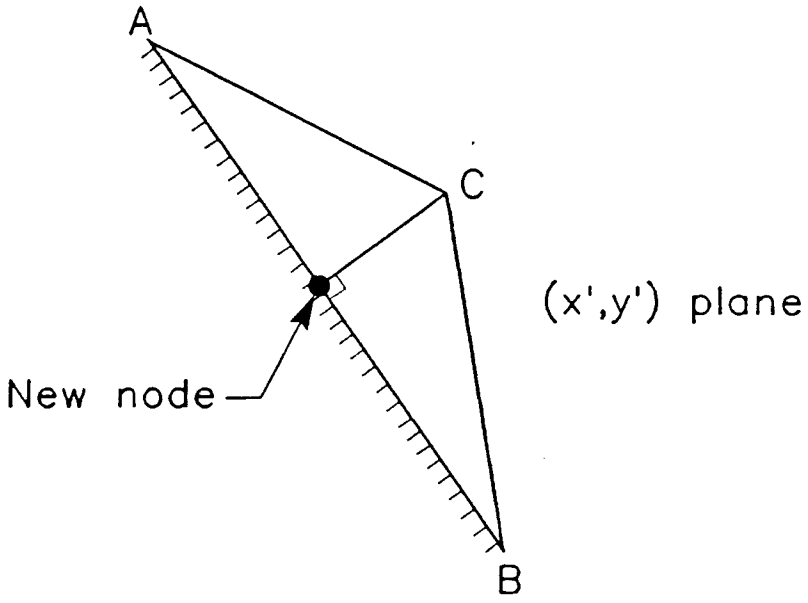

Boundary node addition procedure for a boundary edge.

FIGURE 4

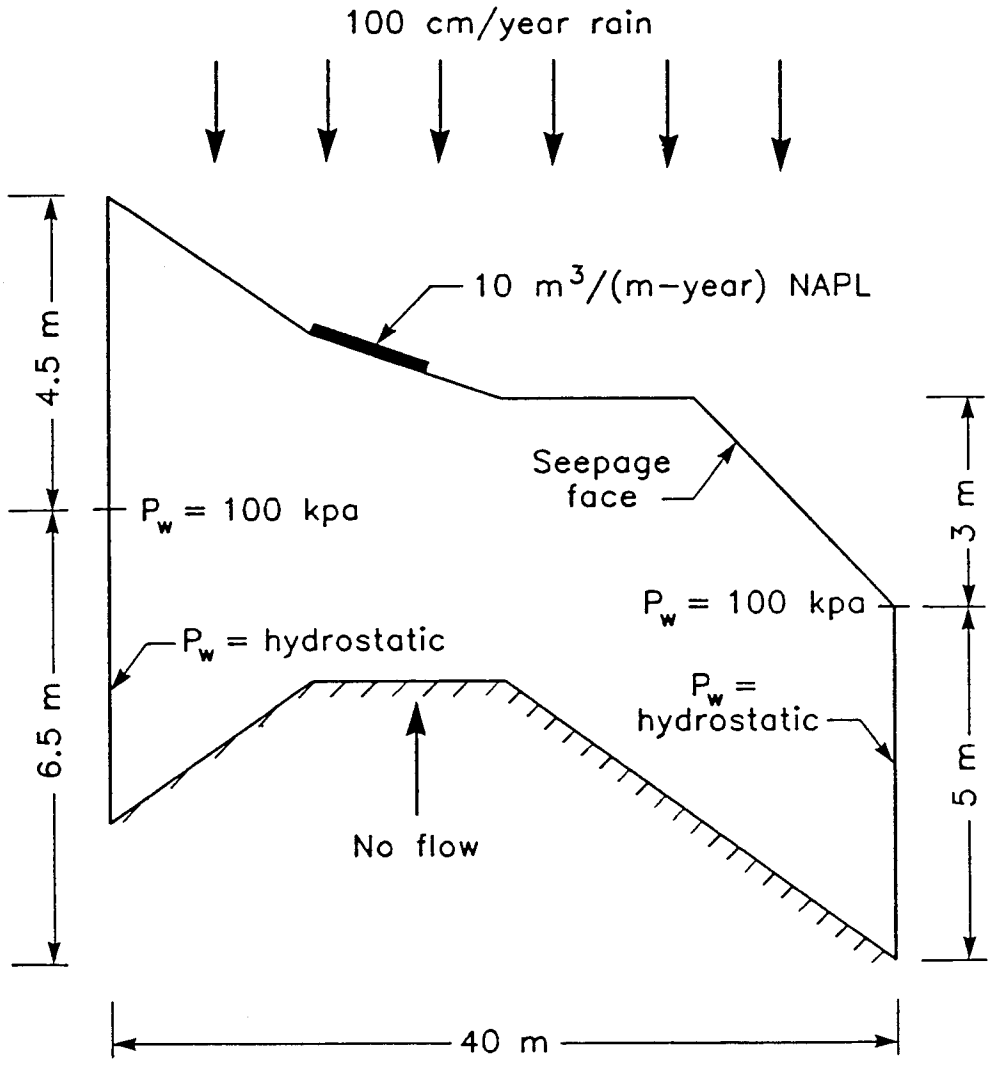

Domain for DNAPL and LNAPL contaminant examples in a homogeneous region.

FIGURE 5

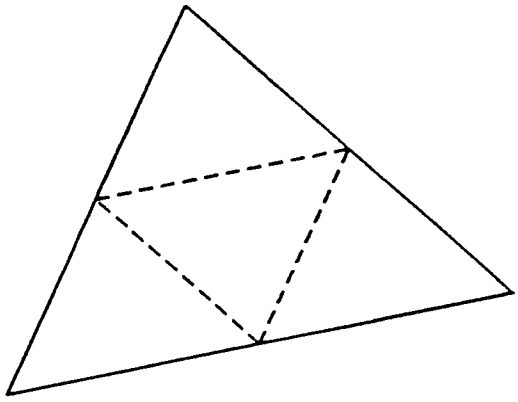

Method for constructing a fine triangulation (dotted plus solid lines) from a coarse triangulation (solid line only).

FIGURE 6(a)

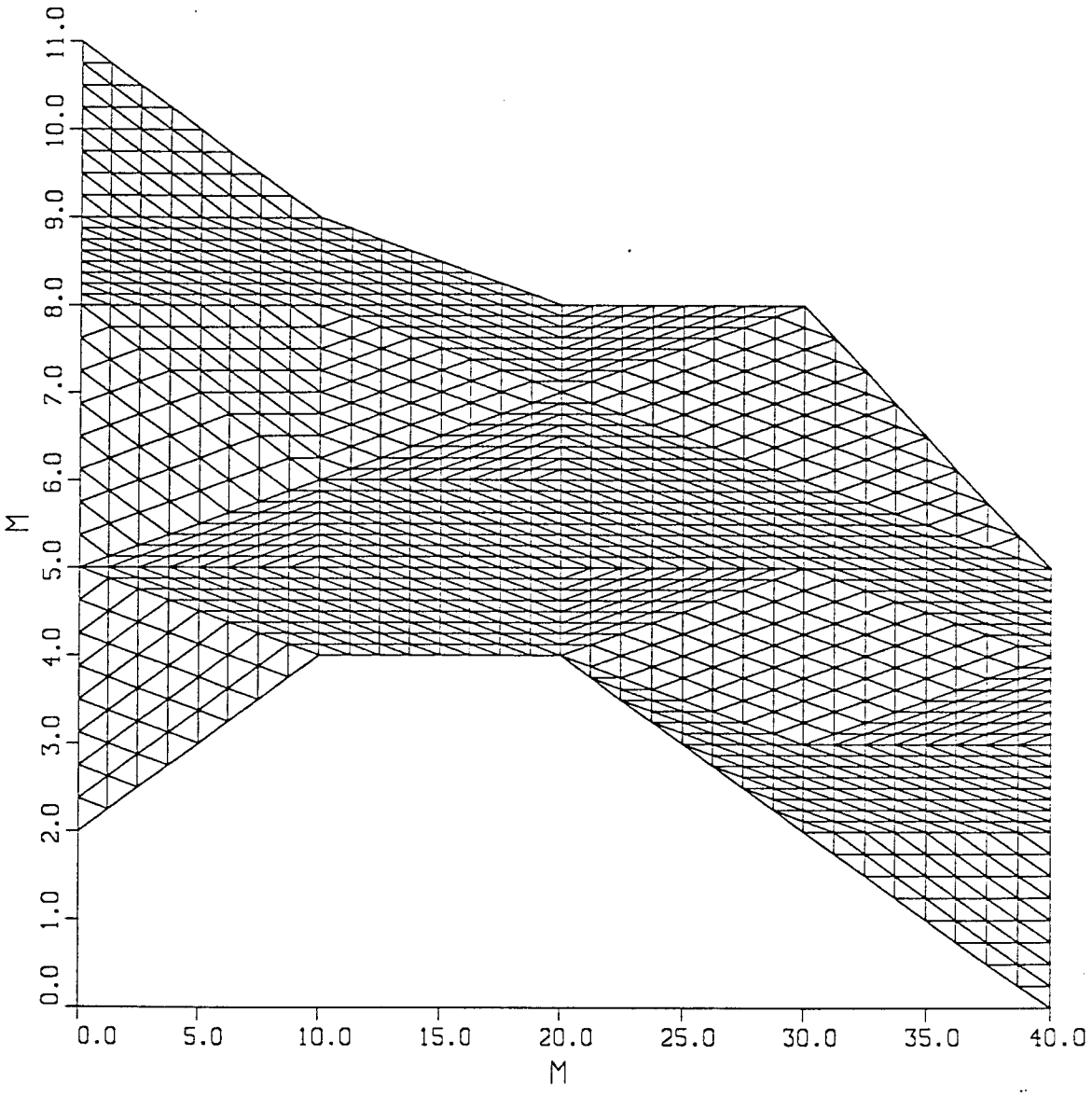

Triangulation for domain of Figure 4

1089 nodes (some negative transmissibilities)

FIGURE 6(b)

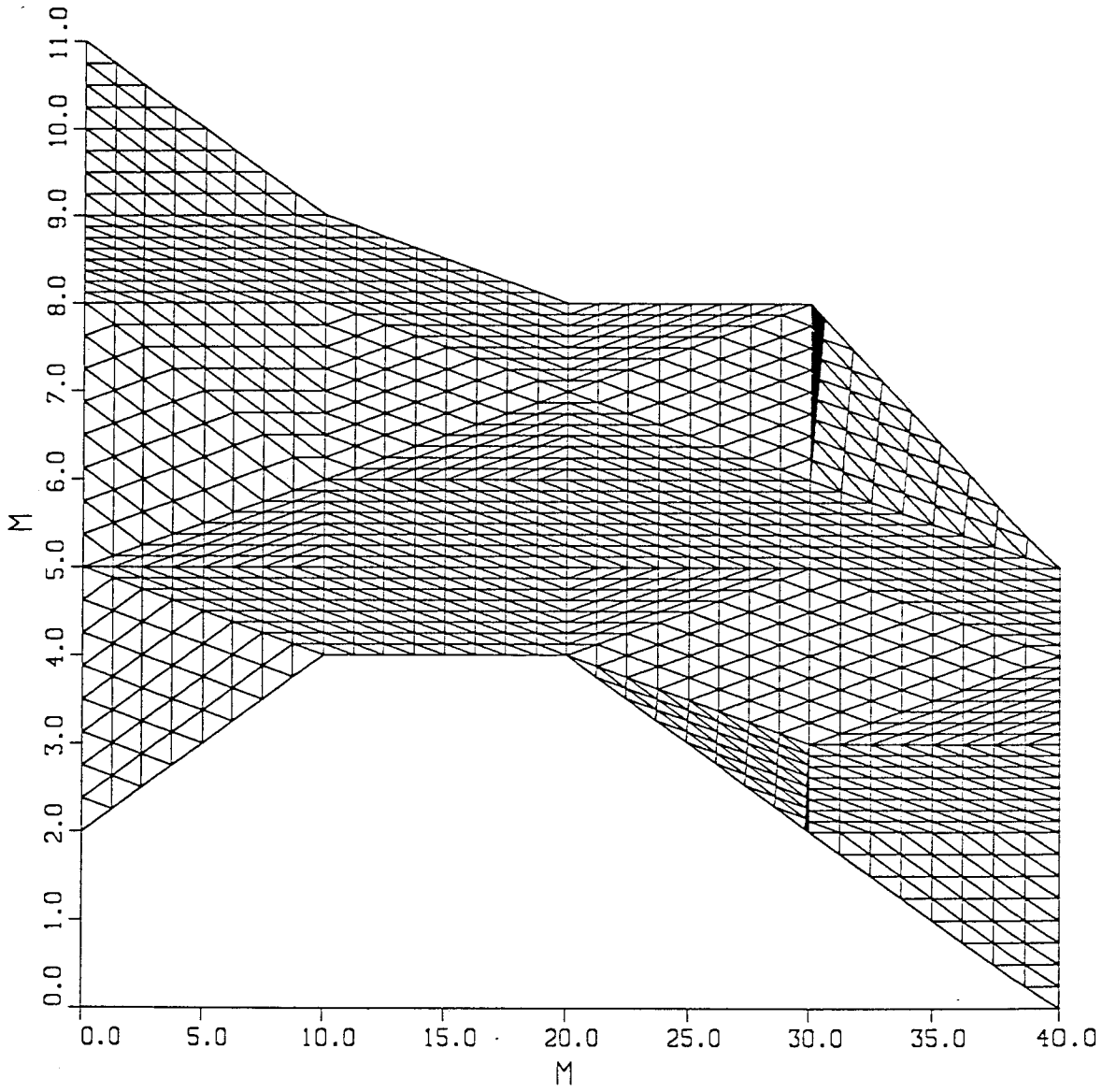

Triangulation for domain of Figure 4

1161 nodes (all positive transmissibilities). Solid colour indicates high density triangulation near extra boundary nodes.

FIGURE 7

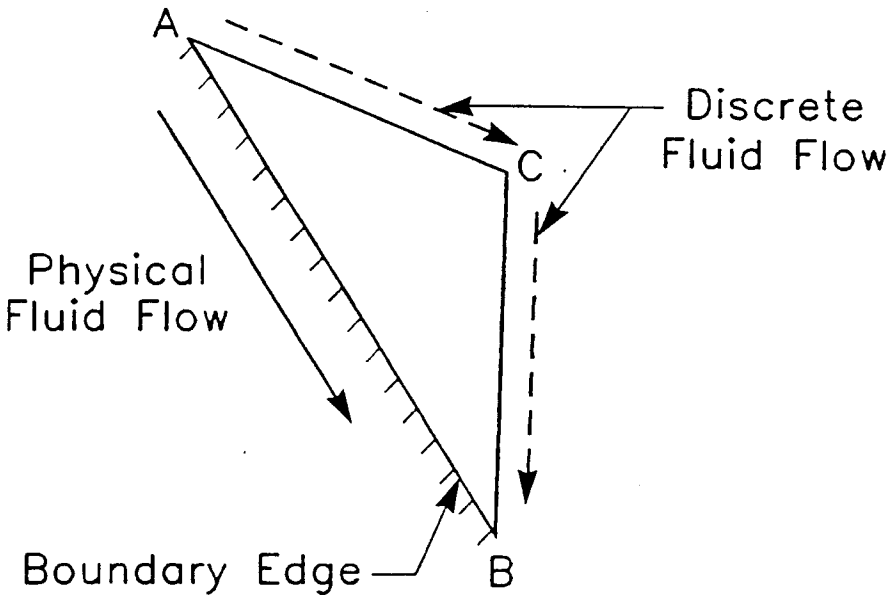

Physical flow path (AC) and discrete flow path ($AB-BC$) when AC has a negative transmissibility.

FIGURE 8(a)

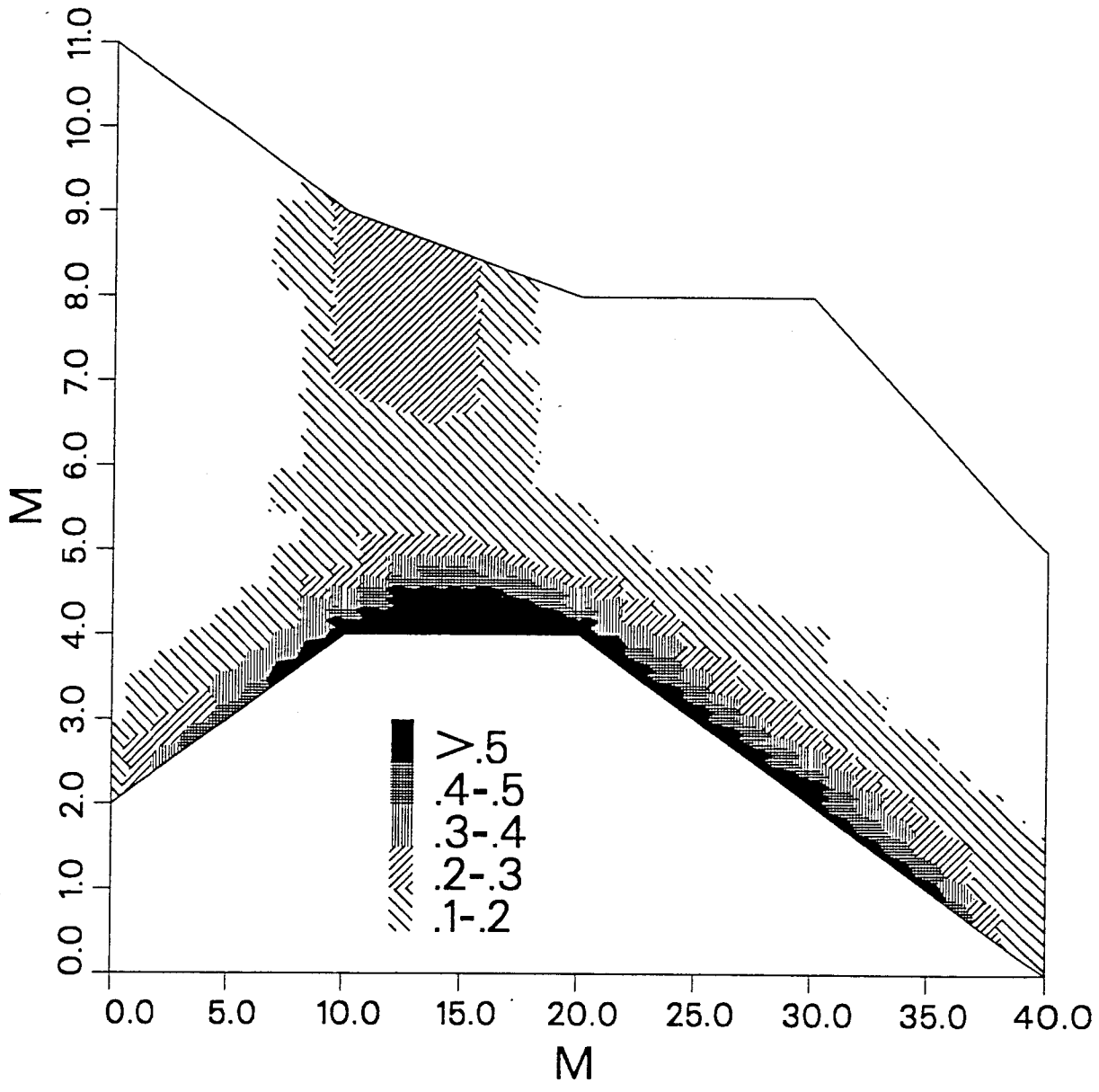

DNAPL saturation values after one year (coarse grid).

Some negative transmissibilities (289 nodes).

FIGURE 8(b)

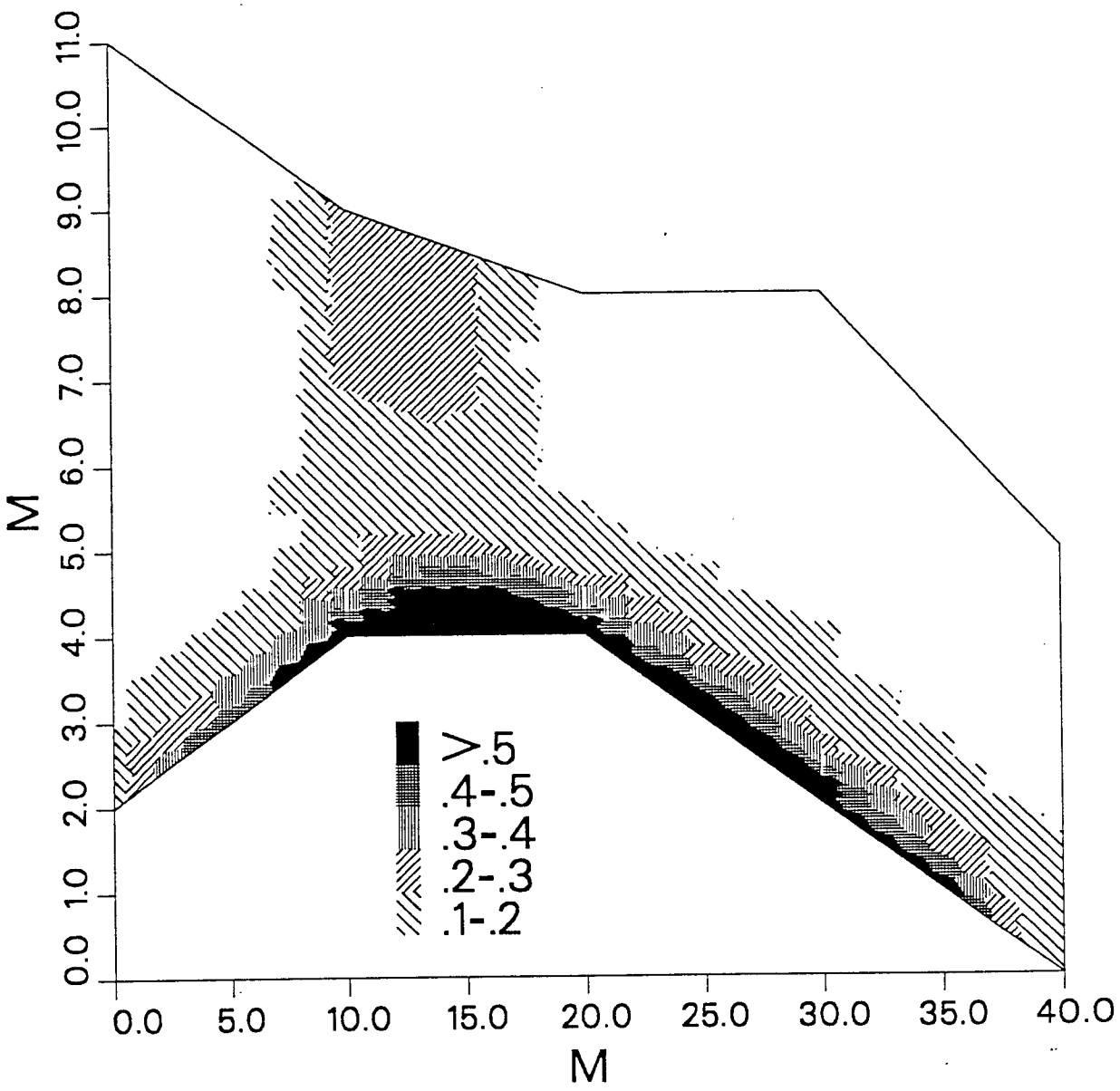

DNAPL saturation values after one year (coarse grid).

All positive transmissibilities (309 nodes).

FIGURE 9(a)

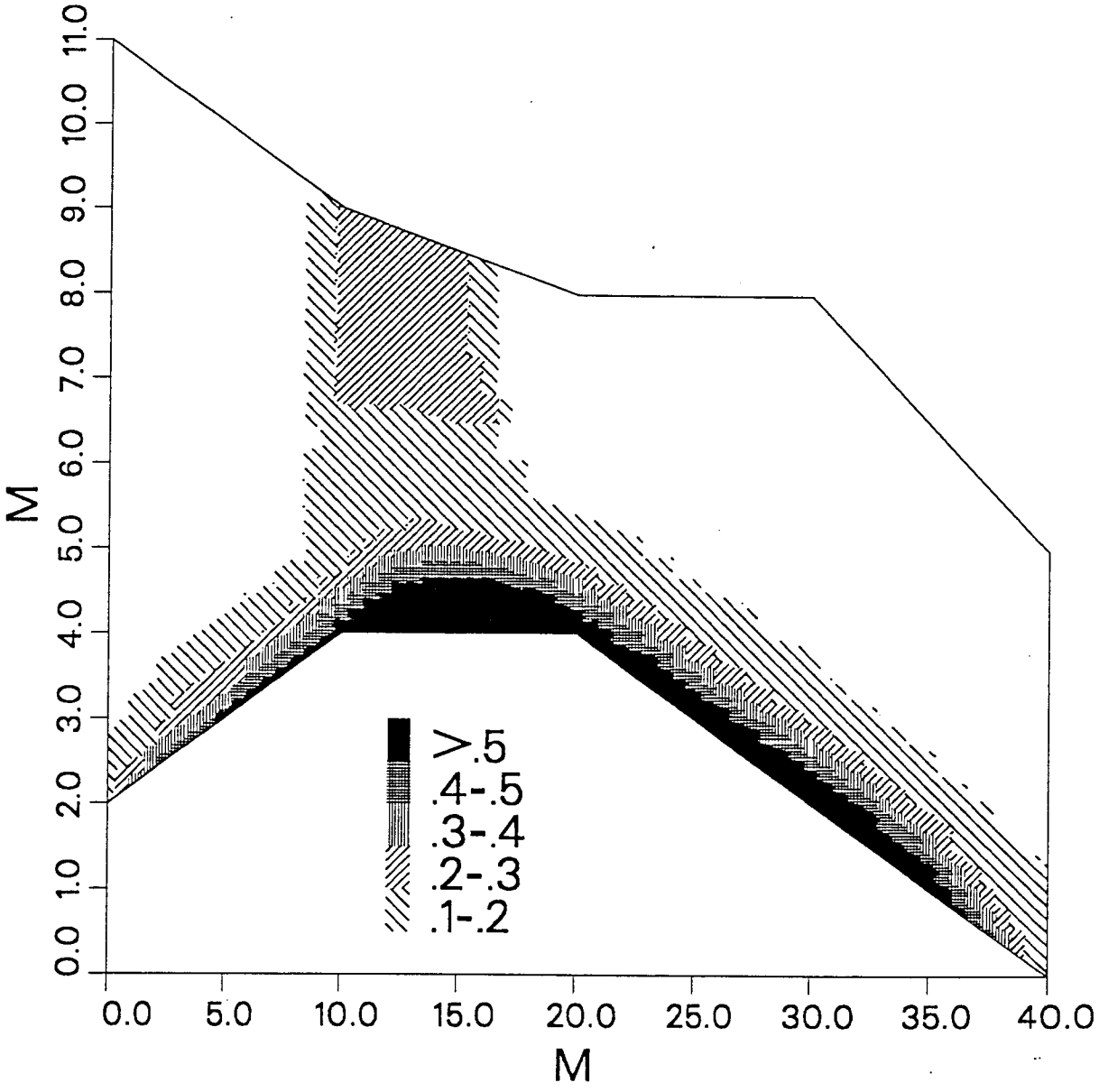

DNAPL saturation values after one year (fine grid).
Some negative transmissibilities (1089 nodes).

FIGURE 9(b)

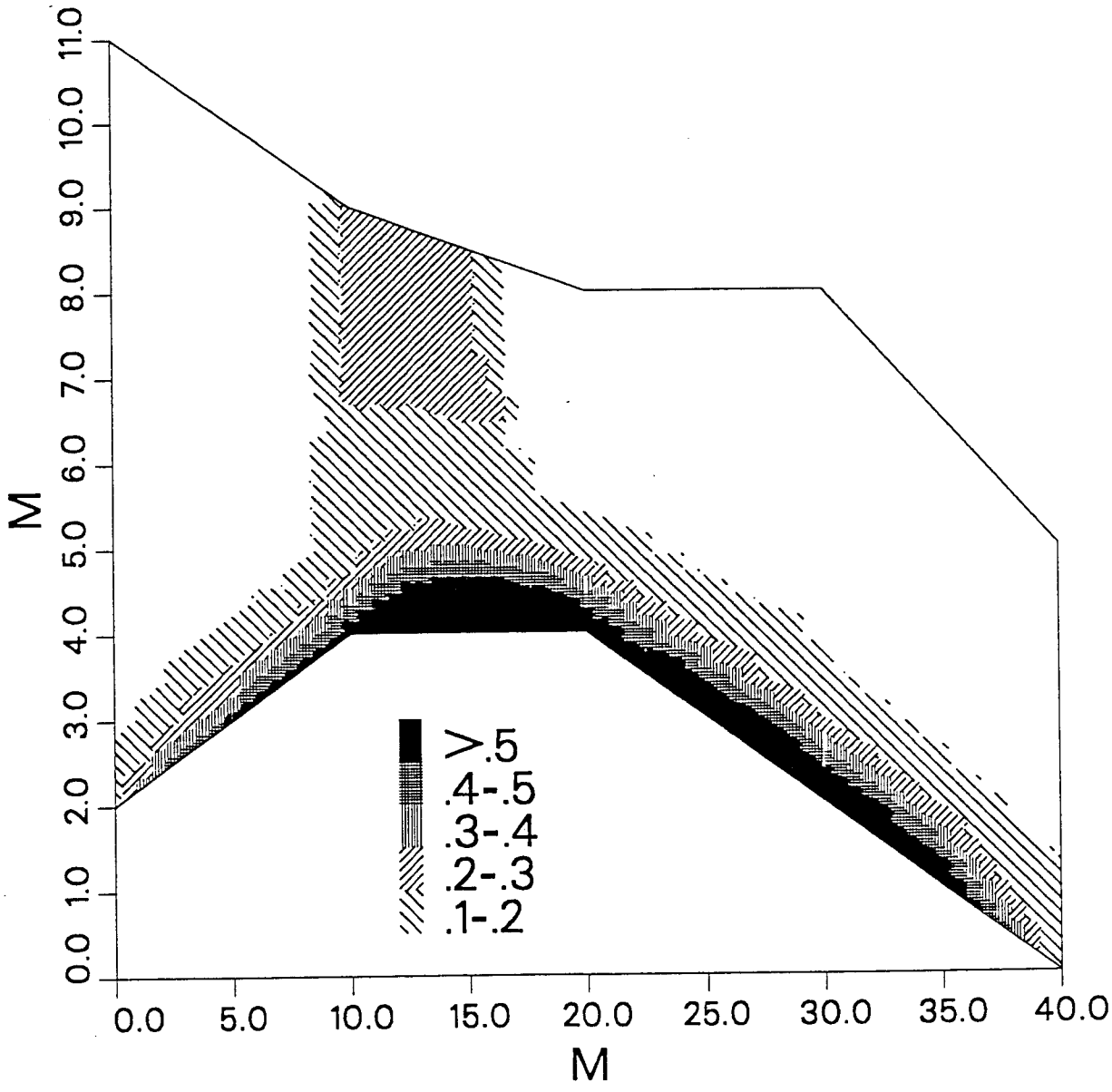

DNAPL saturation values after one year (fine grid).

All positive transmissibilities (1161 nodes).

FIGURE 10(a)

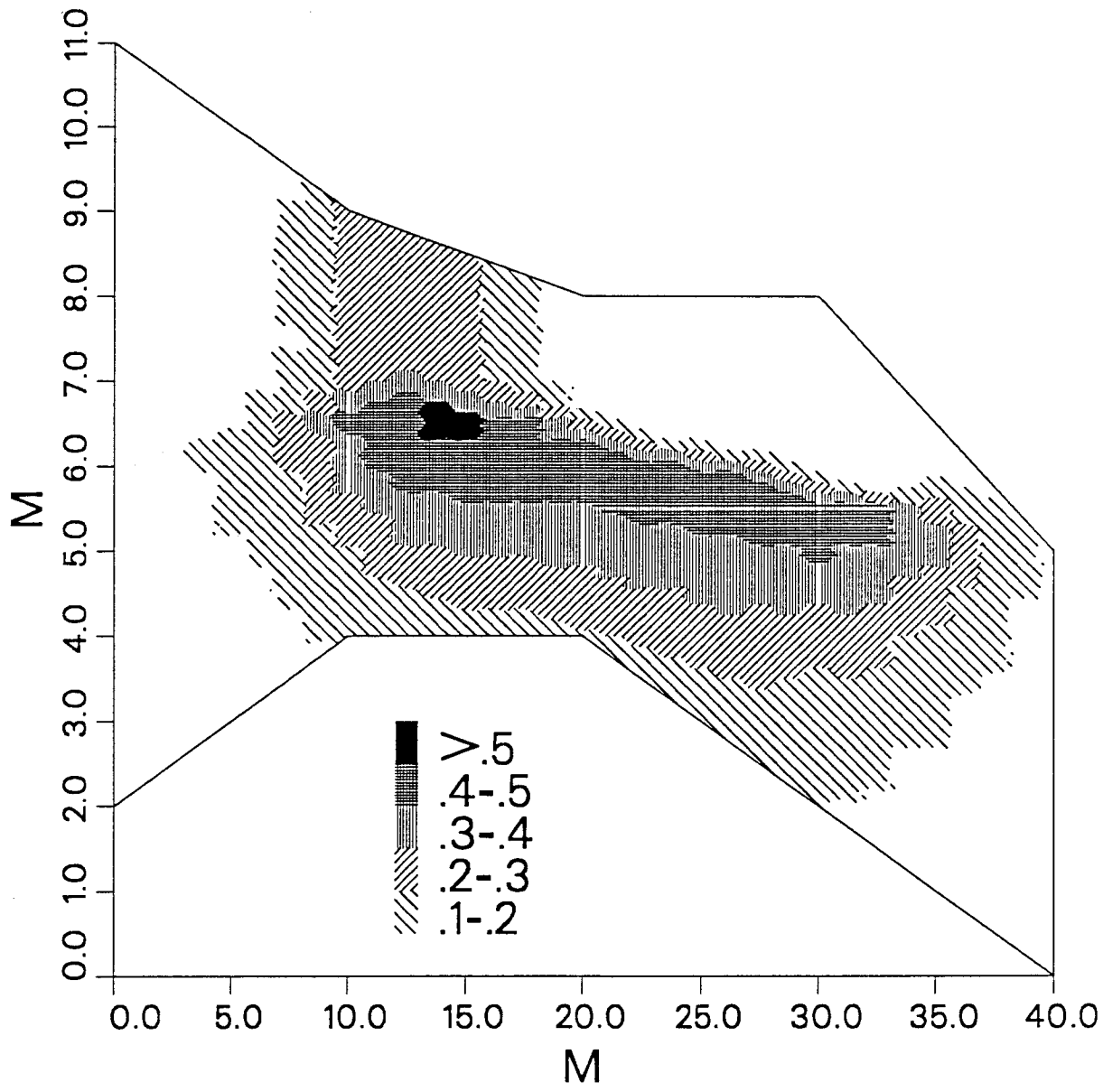

LNAPL saturation values after one year (coarse grid).
Some negative transmissibilities (289 nodes).

FIGURE 10(b)

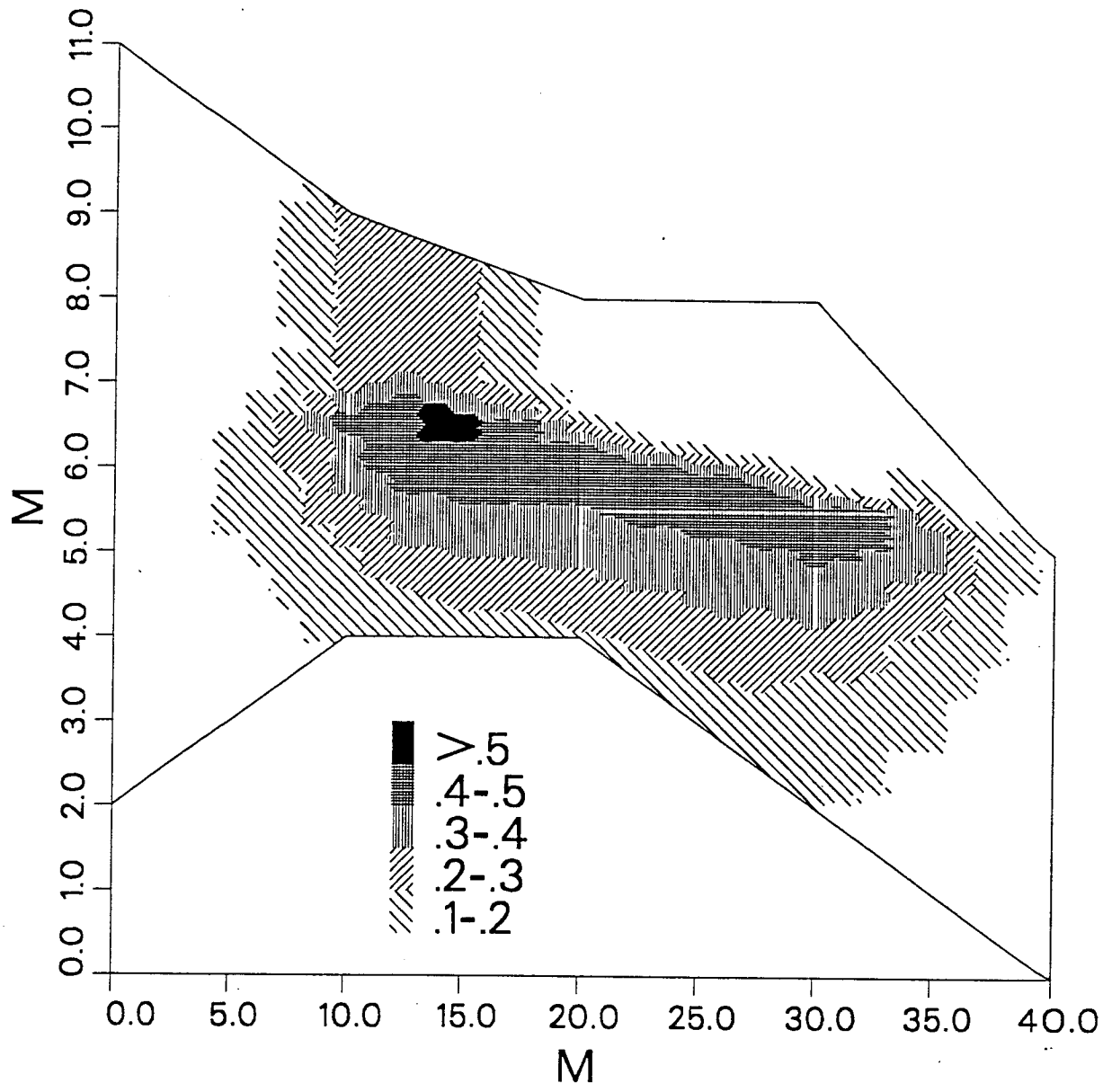

LNAPL saturation values after one year (coarse grid).

All positive transmissibilities (309 nodes).

FIGURE 11(a)

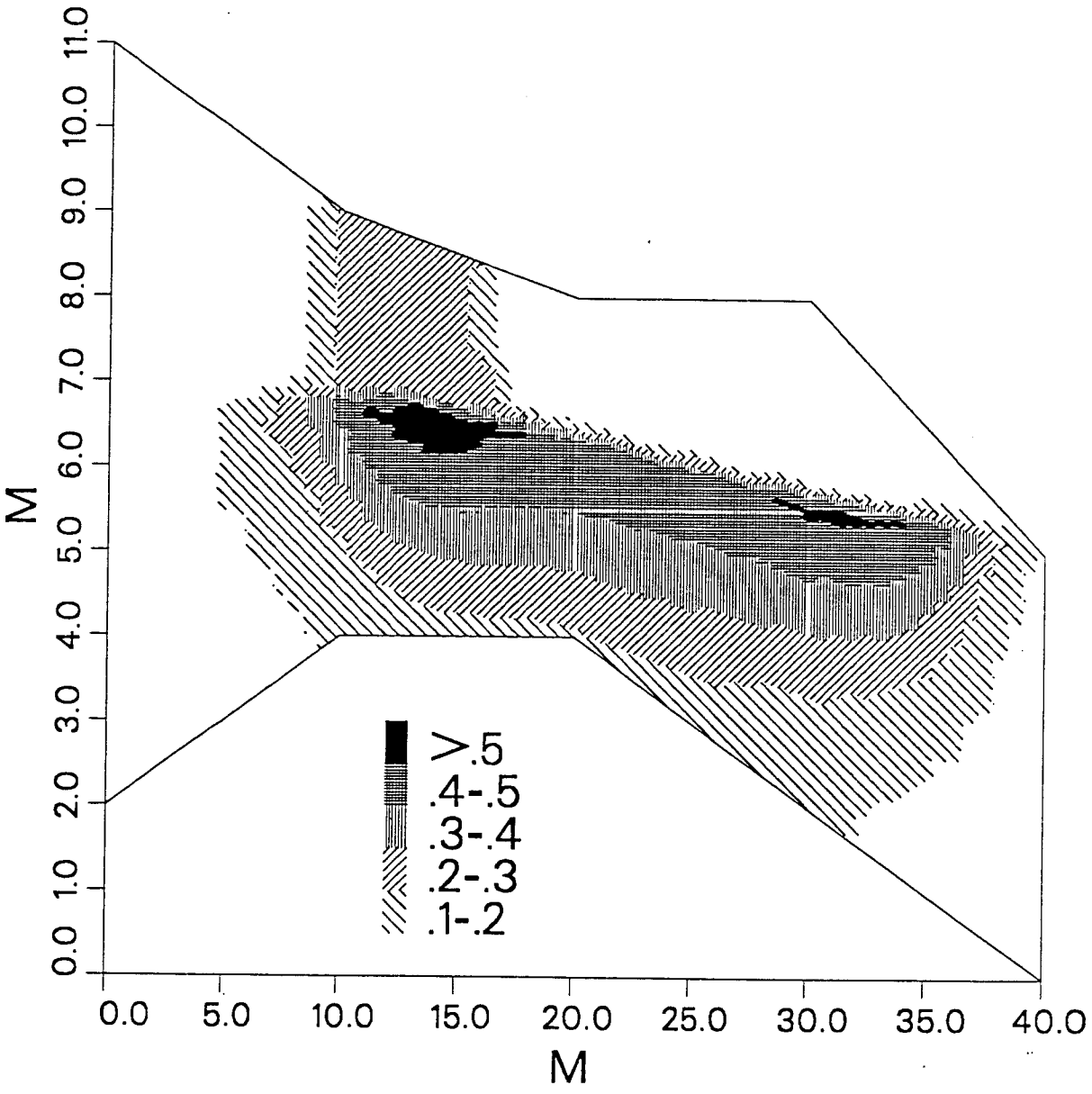

LNAPL saturation values after one year (fine grid).

Some negative transmissibilities (1089 nodes).

FIGURE 11(b)

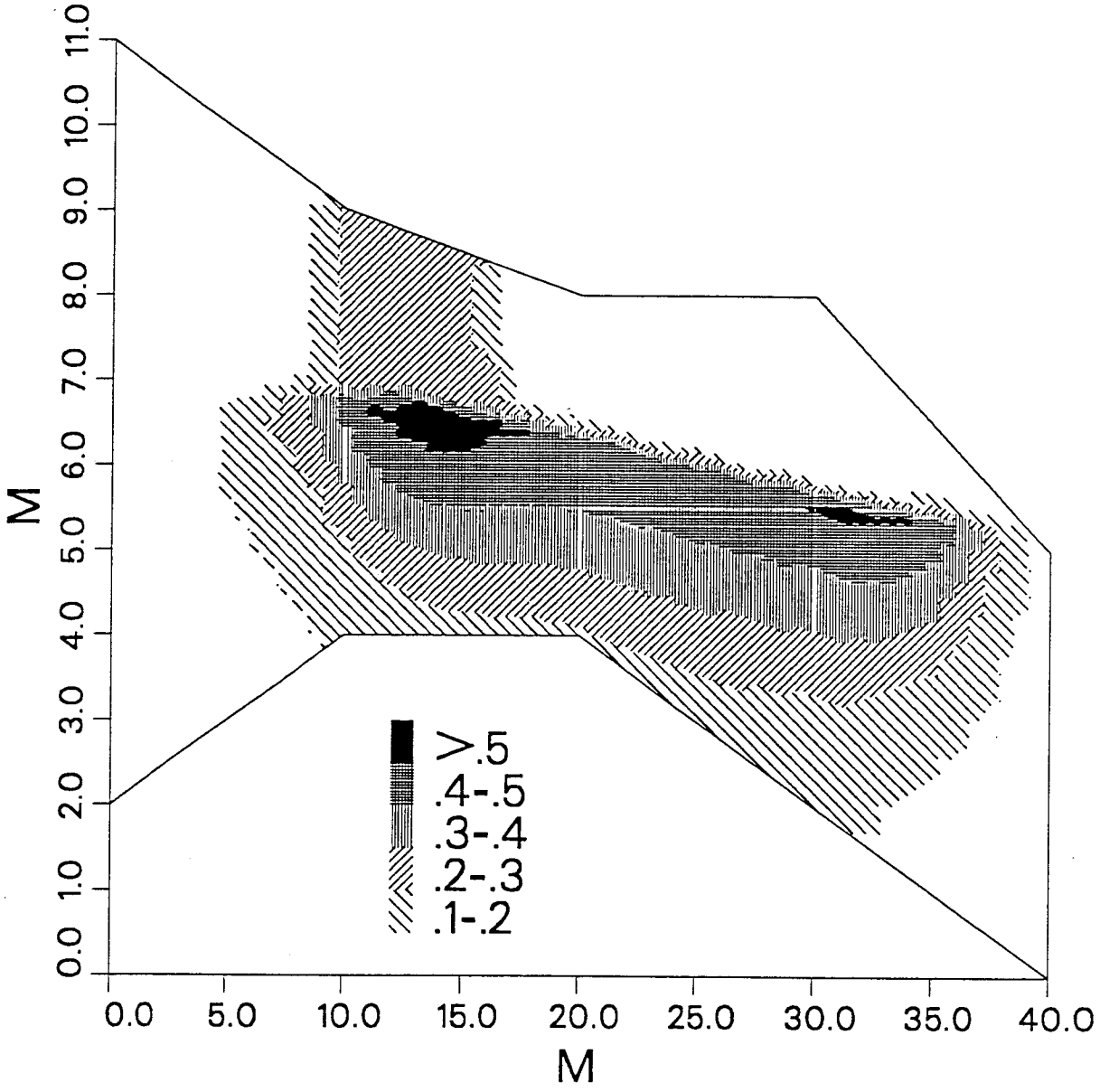

LNAPL saturation values after one year (fine grid).

All positive transmissibilities (1161 nodes).

FIGURE 12

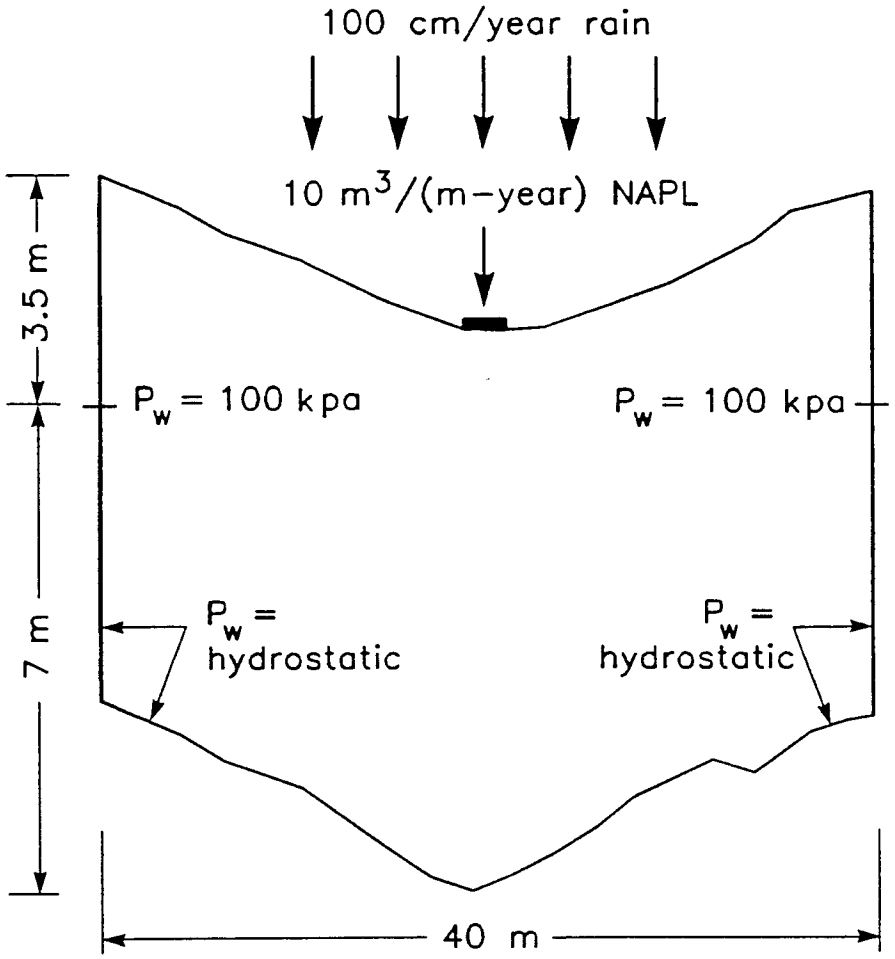

Domain of DNAPL hetrogeneous problem.

FIGURE 13

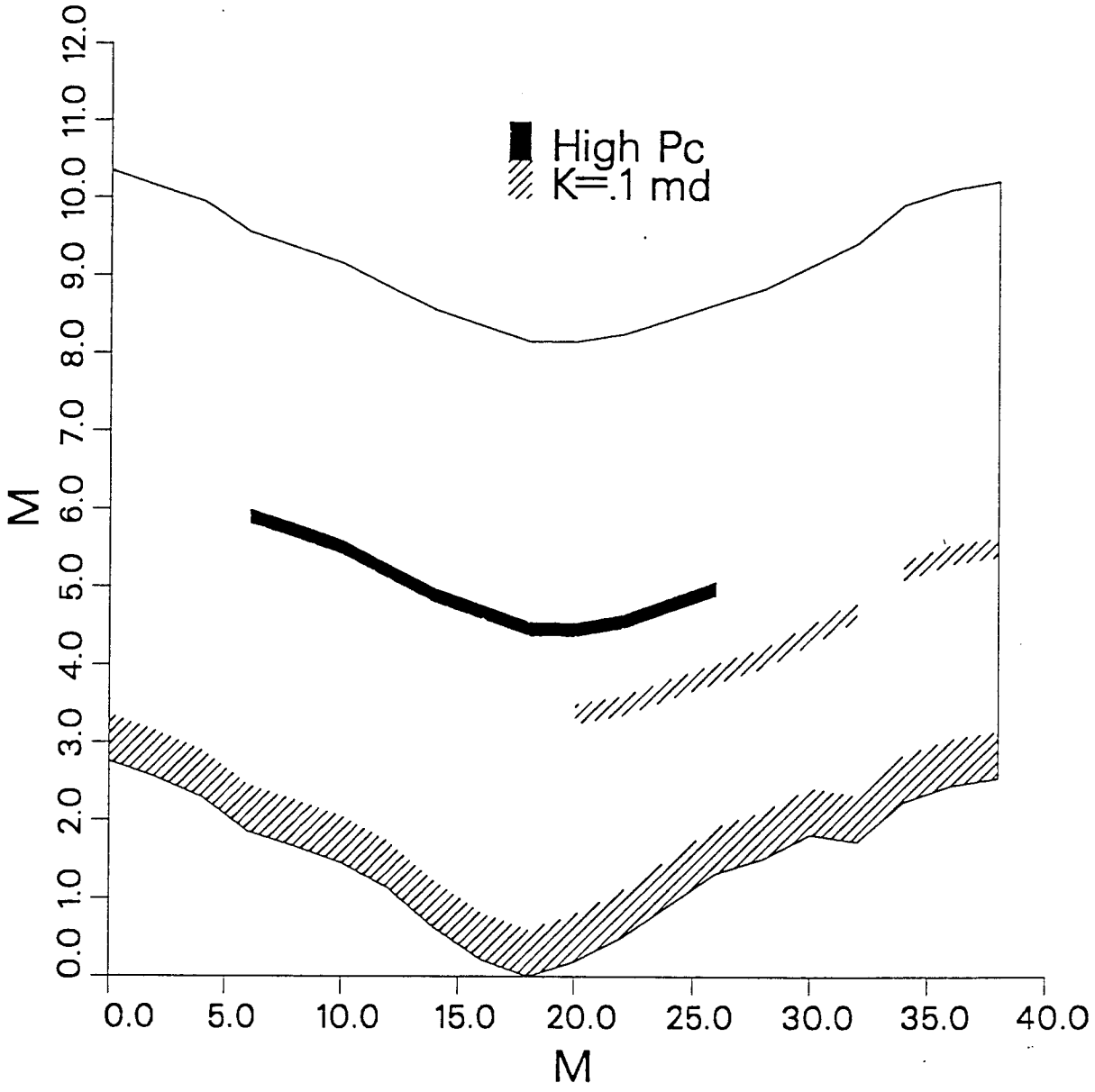

Details of hetrogeneities for Figure 12.

FIGURE 14

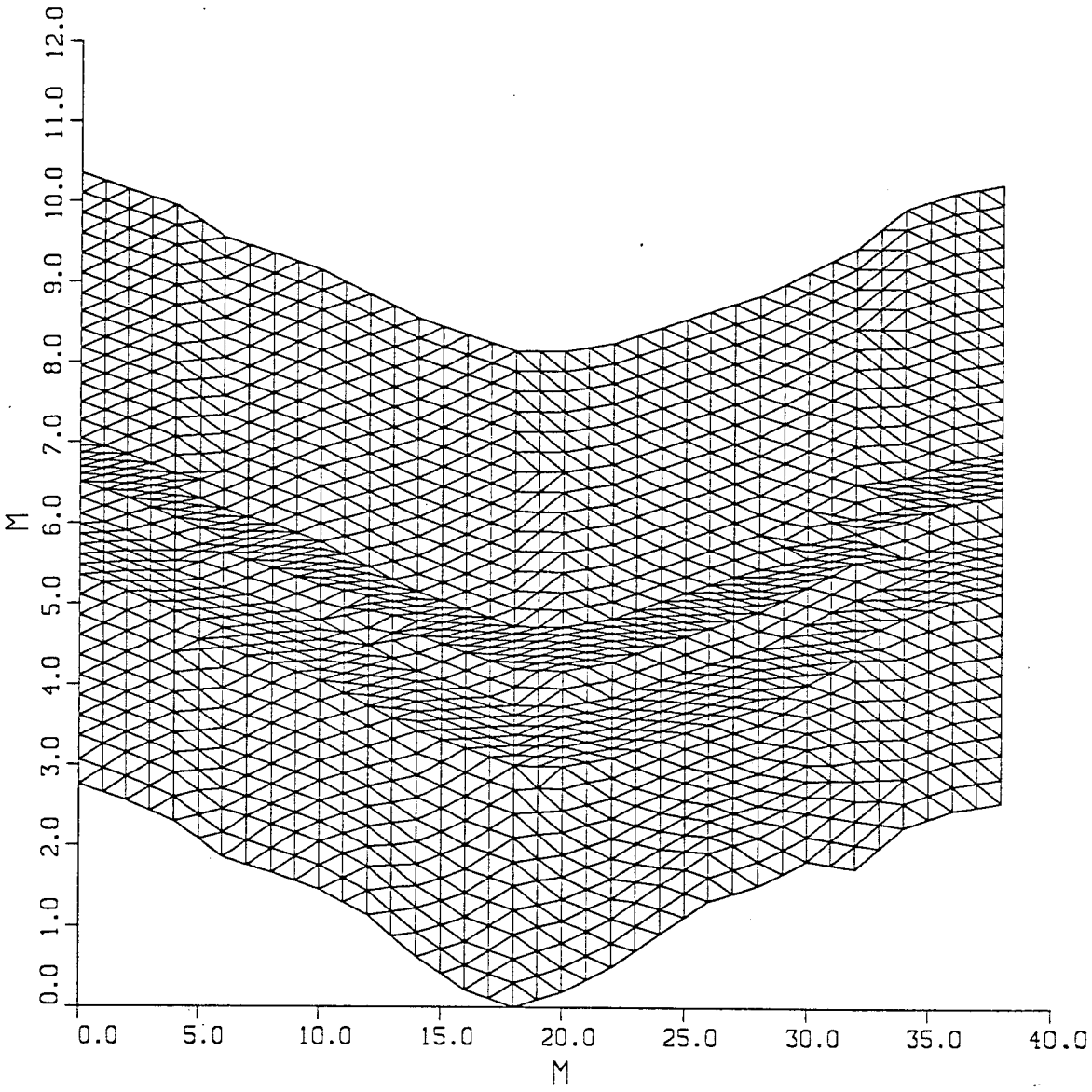

Fine grid triangulation for Figure 12 (1521 nodes).

FIGURE 15(a)

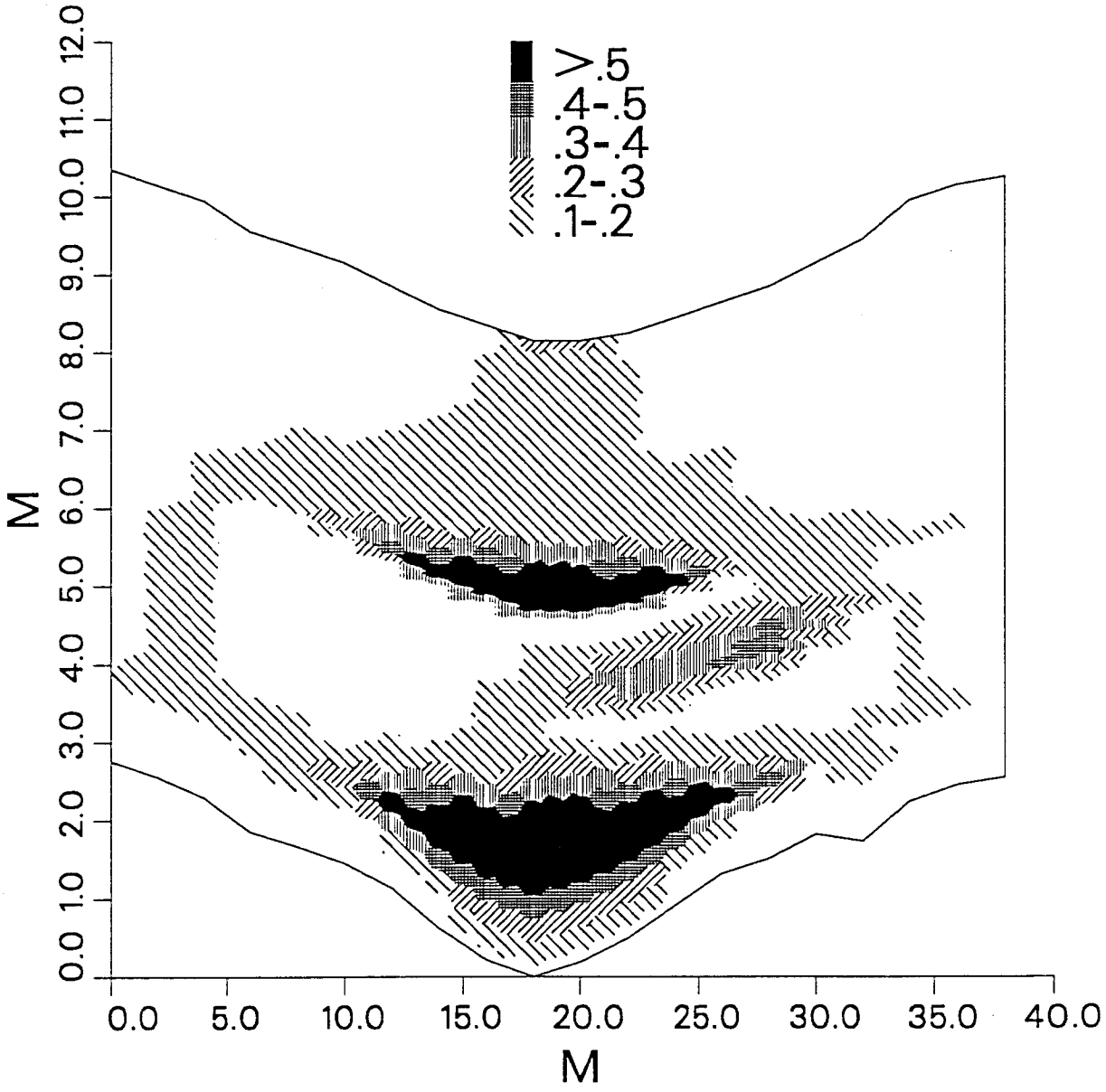

DNAPL saturation values, hetrogeneous problem, after two years.
Coarse grid (400 nodes).

FIGURE 15(b)

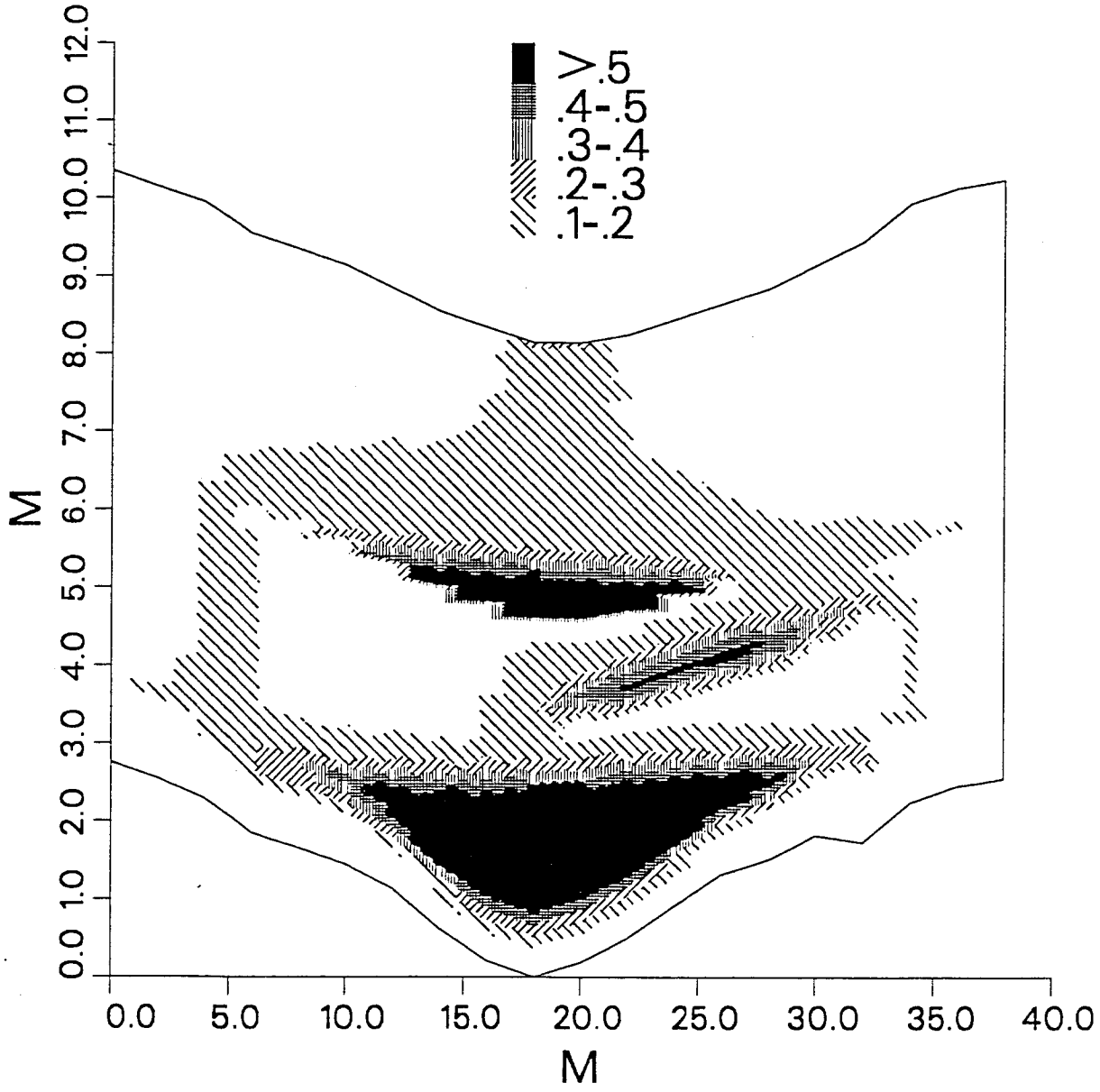

DNAPL saturation values, hetrogeneous problem, after two years.

Fine grid (1521 nodes).